Journal of Solid State Electrochemistry (2023) 27:2337–2345
https://doi.org/10.1007/s10008-023-05515-9

ORIGINAL PAPER

Fabrication of nano-solid spherical Nb_2O_5/nitrogen-doped carbon composite for high-performance sodium-ion battery anodes

Haishan He[1,2] · Yunfei Gan[1,2] · Meiqi Mu[2] · Jujun Yuan[2] · Chao Zhang[2] · Xianke Zhang[2] · Xiaokang Li[1,2] · Xiangdong Ma[2] · Huanjun Yu[2] · Jirong Mou[2] · Jun Liu[2,3]

Received: 7 January 2023 / Revised: 6 April 2023 / Accepted: 15 April 2023 / Published online: 24 April 2023

Abstract

Nano-solid spherical Nb_2O_5/nitrogen-doped carbon (NC) composite is obtained by the hydrothermal method followed by a calcination procedure. The Nb_2O_5/NC composite exhibits good rate performance and sustainable cyclic stability (144 mAh g^{-1} at 1000 mAh g^{-1} upon 2000 charge–discharge cycles) as an anode material in Na-ion batteries (SIBs). The excellent performance of the Nb_2O_5/NC composite is attributed to its unique nanosphere structure, in which Nb_2O_5 nanocrystals embedded in porous NC matrix can restrain agglomeration of Nb_2O_5 nanocrystals and ensure electrolyte accessibility, and the NC matrix can provide effective active sites and increase ions/electrons transfer. This work offers a new method to fabricate nano-solid spherical Nb_2O_5/NC composite with good Na^+ storage property, which can be extended for synthesizing other metal oxide/NC composite as SIB anode.

Introduction

As an effective energy storage device, LIBs are extensively used in 3C digital products and new energy automobile [1–4]. However, lithium resources are limited, which limits the application of LIBs in massive scale energy storage [5]. Therefore, it is urgent to develop another energy storage device to replace LIBs, which can be applied in the large-scale energy storage [6, 7]. In recent years, sodium-ion batteries (SIBs) with similar chemical properties for LIBs have attracted the attention of the majority of scientific researchers due to their abundant resources, low cost, and environmental friendliness [8–11]. However, compared with the ionic radius of lithium ion ($r = 0.076$ nm), the ionic radius of sodium ion ($r = 0.113$ nm) is at least 35% larger [5, 12], which leads to the problem of volume effect, so it is necessary to seek more efficient electrode materials.

As an intercalation anode material [13], Nb_2O_5 has a theoretical specific capacity (200 mAh g^{-1}) with low-volume expansion, high-rate capability resulting from a pseudocapacitive Li/Na storage mechanism. However, Nb_2O_5 is a semiconductor (with a band gap ranging from 3.2 to 4 eV) with poor electrical conductivity ($\approx 3.4 \times 10^{-6}$ S cm^{-1} at 300 K) [14]. In order to solve the problem of low electrical conductivity, constructing Nb_2O_5/C composites is proved to be an effective method [15]. Particularly, Nb_2O_5/C nanostructures as electrode materials can cut down the diffusion separation of ions, enhance the electrical conductivity, and ultimately improve their electrochemical performance [16]. For example, Kim et al. [17] synthesized an ordered mesoporous Nb_2O_5/C composite structure, which displayed a invertible capacity of 175mAh g^{-1} and splendid cycle stability for SIBs. Mai et al. [18] proposed an effective method to establish three typical carbon-constrained Nb_2O_5 (TT-Nb_2O_5@C, T-Nb_2O_5@C, and

✉ Jujun Yuan
yuanjujun123@163.com

✉ Xiaokang Li
lixiaokang@gnnu.edu.cn

✉ Huanjun Yu
406385064@qq.com

[1] College of Chemistry and Chemical Engineering, Gannan Normal University, Ganzhou 341000, People's Republic of China

[2] Key Laboratory of New Energy Materials and Low Carbon Technologies, College of Physics and Electronics, Gannan Normal University, Ganzhou 341000, People's Republic of China

[3] School of Materials Science and Engineering, South China University of Technology, Guangzhou 510641, People's Republic of China

H-Nb_2O_5) nanoparticles through mismatched coordination reactions in a solvothermal process. It was found that the obtained T-Nb_2O_5@C nanoparticles exhibited better performance than TT-Nb_2O_5@C and H-Nb_2O_5@C nanoparticles. Vicentini et al. [19] reported a method for preparing nanostructured porous electrodes by electrospraying niobium pentoxide nanoparticles on wound multi-walled carbon nanotubes. This method not only can improve electrical conductivity and chemical stability of the niobium pentoxide, but also avoid reassociation and deactivation of Nb_2O_5 nanoparticles. In addition, Yuan et al. [20] synthesized a unique pomegranate-like Nb_2O_5@NC material by hydrothermal method and nitrogen-doped carbon coating process, which exhibited excellent cycle stability for Na-ion batteries anode. The above electrochemical results of Nb_2O_5/C nanocomposites show that Nb_2O_5/C composites with different structures and morphologies have an impact on their electrochemical properties. Therefore, it is worth continuing to seek a simple method for designing and synthesizing Nb_2O_5/C composites to obtain anode materials with excellent sodium storage properties [21, 22].

Therefore, for the first time, we designed the nano-solid spherical Nb_2O_5/NC composite by a simple hydrothermal method followed by a simple calcination process. For Na storage, the Nb_2O_5/NC composite possesses the advantages of Nb_2O_5 nanocrystals embedded in porous NC matrix restraining agglomeration of Nb_2O_5 nanocrystals and ensuring electrolyte accessibility and the NC matrix providing effective active sites and increasing ions/electrons transfer. As anode material in SIBs, the Nb_2O_5/NC composite electrode exhibits excellent rate performance and cyclic stability (144 mAh g^{-1} at 1000mAh g^{-1} after 2000 cycles).

Experimental

Synthesis of Nb_2O_5/NC composites

Two hundred mg of niobium oxalate hydrate was dissolved in 20 mL of absolute ethanol to get solution 1 and 200 mg of dopamine hydrochloride was dissolved in 20 mL of deionized water to form solution 2. The mixed solutions were obtained by mixing solutions 1 and 2 with stirring for 1 h. Whereafter, the mixed solution was put into Teflon lined stainless steel autoclave and reacted at 180 °C for 12 h. The obtained Nb-polydopamine precursor was washed with distilled water and absolute ethanol and dried at 60 °C for 12 h. The Nb-polydopamine precursor was put into a tube furnace, heated to 600 °C at 3 °C/min, and kept for 2 h under Ar atmosphere for obtaining the Nb_2O_5/NC composite material.

Material characterization

The crystal phase and chemical composition of Nb_2O_5/NC composites were detected by XRD (DX2700) and XPS (Escalab250Xi), respectively. The morphology and structure of Nb_2O_5/NC composites were determined by SEM (SU8010, Hitachi) and TEM (JEOL JEM-3000F), respectively. The weight ratio of Nb_2O_5 in the Nb_2O_5/NC composites was tested by thermogravimetric analysis (TGA, TA-209F3). The BET surface area of Nb_2O_5/NC composites was measured by Quadrachrome Adsorption Instrument.

Electrochemical measurements

The electrochemical performance of Nb_2O_5/NC composites was tested employing a CR2032 coin cell battery. The active material, carbon black, and sodium alginate (dissolved in water) in a ratio of 7:2:1 were mixed in the an agate bowl. And then the slurry was coated on the copper foil and dried at 80 °C overnight. These half-cells were assembled in a glove box which was filled with argon as the working gas. Sodium sheet was used as the counter electrode, and 1 M $NaClO_4$ EC/PC (1:1) solution with 10% FEC was used as the electrolyte. Constant current charge/discharge tests were performed using a NEWARE battery tester (voltage range at room temperature was 0.01–3.0 V). Cyclic voltammetry (CV) and electrochemical impedance spectra (EIS) were obtained using versatile multichannel potentiostat (VMP3). The voltage window of cyclic voltammetry was 0.01–3.0 V (relative to Na/Na^+), the frequency range of electrochemical impedance was 200 mHz to 200 kHz, and the AC signal amplitude was 0.5 mV.

Results and discussion

The precursors were annealed under argon and air atmospheres to obtain Nb_2O_5/NC composite and pure Nb_2O_5. The crystalline structure of Nb_2O_5/NC composite was characterized by X-ray diffraction (XRD) as shown in Fig. 1. Figure 1a exhibited the XRD pattern of the Nb_2O_5/NC composite. It is easy to discover that all the diffraction peaks are corresponded to hexagonal Nb_2O_5 (JCPDS card No.7–61). As shown in Fig. 1b, all the diffraction peaks for pure Nb_2O_5 are also corresponded to hexagonal Nb_2O_5 (JCPDS card No.7–61). Figure 1c is the TGA diagram of the Nb_2O_5/NC composite. It can be seen from the figure that the mass loss of the Nb_2O_5/NC composite is 27.5% at 750 °C, and then the mass remains unchanged, indicating that the mass of Nb_2O_5 in the Nb_2O_5/NC composite is

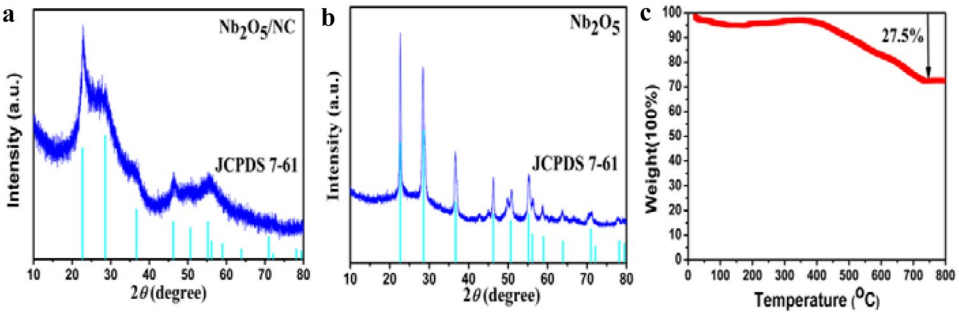

Fig. 1 **a** XRD of Nb_2O_5/NC composites; **b** XRD of pure Nb_2O_5; **c** TGA analysis of Nb_2O_5/NC composites

72.5%. Figure 2 shows the BET characterization of Nb_2O_5/NC composites. It is obvious that the specific surface area of the material is 46.1 m^2 g^{-1} (Fig. 2a). The pore sizes of the Nb_2O_5/NC composite (Fig. 2b) were mainly represented at 4.202, 17.5, and 21 nm. The special mesoporous architecture can ensure enough contact area between electrodes and electrolyte.

The elemental composition analysis of Nb_2O_5/NC composites was carried out by XPS. The Nb 3d spectrum of the Nb_2O_5/NC composite with two signal peaks at 207.15 and 209.2 eV is shown in Fig. 2c, which were in tune with Nb $3d_{5/2}$ and Nb $3d_{3/2}$, respectively. Figure 2d is the C 1 s spectrum of the Nb_2O_5/NC composite, in which signal peak at 284.8 and 286.2 eV corresponds to C–C and C-O, respectively. Figure 2e shows the O 1 s spectrum of the Nb_2O_5/NC composite, whose signal peak at 530.5, 530.7, and 532.3 eV conform to Nb–O, C-O, and C = O, respectively [20, 23]. Figure 2f is the N 1 s spectrum of the Nb_2O_5/NC composite, in which two signal peaks at 398.6 and 400.6 eV correspond to pyridine-N and pyrrole-N, respectively [24].

The morphologies of the Nb precursor, Nb_2O_5/NC composites, and pure Nb_2O_5 have been characterized by SEM. As shown in Fig. S1a, b, the Nb precursor shows nano-solid spherical morphology with diameter of 400–600 nm. After annealing treatments, it can be seen from Fig. 3a the Nb_2O_5/NC composites remain nano-solid spherical morphology. As displayed in the Fig. S1c, d, the pure Nb_2O_5 also keeps the nano-solid spherical morphology. Energy dispersive system (EDS) mapping of Nb_2O_5/NC composites (Fig. 3c) proves that carbon (C), oxygen (O), niobium (Nb), and nitrogen (N) are uniformly distributed in the surface of the material. The microstructure of the Nb_2O_5/NC composites is researched by TEM. As depicted by TEM observation in Fig. 4b, lots of Nb_2O_5 nanocrystals (5–10 nm) were embedded in carbon matrix. As shown in the HRTEM image (Fig. 4c), it can be found that the interplanar spacing of 0.312 nm corresponds to the (100) plane of Nb_2O_5. Figure 4d shows EDS mapping images of Nb_2O_5/NC composites under transmission electron microscope. It can be observed that the C, O, Nb, and N are uniformly distributed within Nb_2O_5/NC composites, implying the Nb_2O_5 nanocrystals are uniformly distributed in the NC matrix. Thus, it can be proved that the Nb_2O_5/NC composite has been successfully prepared.

The electrochemical performance of the Nb_2O_5/NC composite as the anode of SIBs was tested by cyclic voltammogram (CV) and galvanostatic cycling and electrochemical impedance measurements. Figure 5a shows the first five CV curves of the Nb_2O_5/NC composite at 0.2 mV s^{-1}. The first curve shows two irreversible reductive peaks at 1.0 and 0.24 V, but they disappear in the subsequent curve, which can be attributed to the formation of the SEI film, the irreversible Na-ion insertion in the surface groups of carbon as well as organic electrolyte decomposition [25, 26]. The latter four cyclic voltammetry curves basically overlap, indicating that the Nb_2O_5/NC composite exhibits reversibility and stable cycling. Figure 5b shows the first three charge–discharge curves at 1000 mAh g^{-1}. The initial charge–discharge capacities are 32 mAh g^{-1} and 108 mAh g^{-1}, respectively, and the coulombic efficiency is 30%. The low coulombic efficiency of the Nb_2O_5/NC composite can be ascribed to SEI film formation and the irreversible Na-ion insertion in the surface groups of carbon as well as organic electrolyte decomposition [27]. When the battery is cycled to the 10th time, the charge and discharge capacities are 65 mAh g^{-1} and 67 mAh g^{-1}, respectively, and the coulomb efficiency reaches 97% (as shown in Fig. 5c), and the subsequent coulomb efficiency remains 97% and the foregoing, indicating that the Nb_2O_5/NC composite shows good reversible properties. Figure 5c shows the cycling performance of the Nb_2O_5/NC composite. After 2000 cycles at a current density of 1000 mA g^{-1}, the specific capacity of the battery is 144 mAh g^{-1} and the charge–discharge efficiency remains around 100%. Figure 5d shows the rate performance of Nb_2O_5/NC composite and Nb_2O_5. As shown in Fig. 5d, the specific capacity of Nb_2O_5/NC composite is

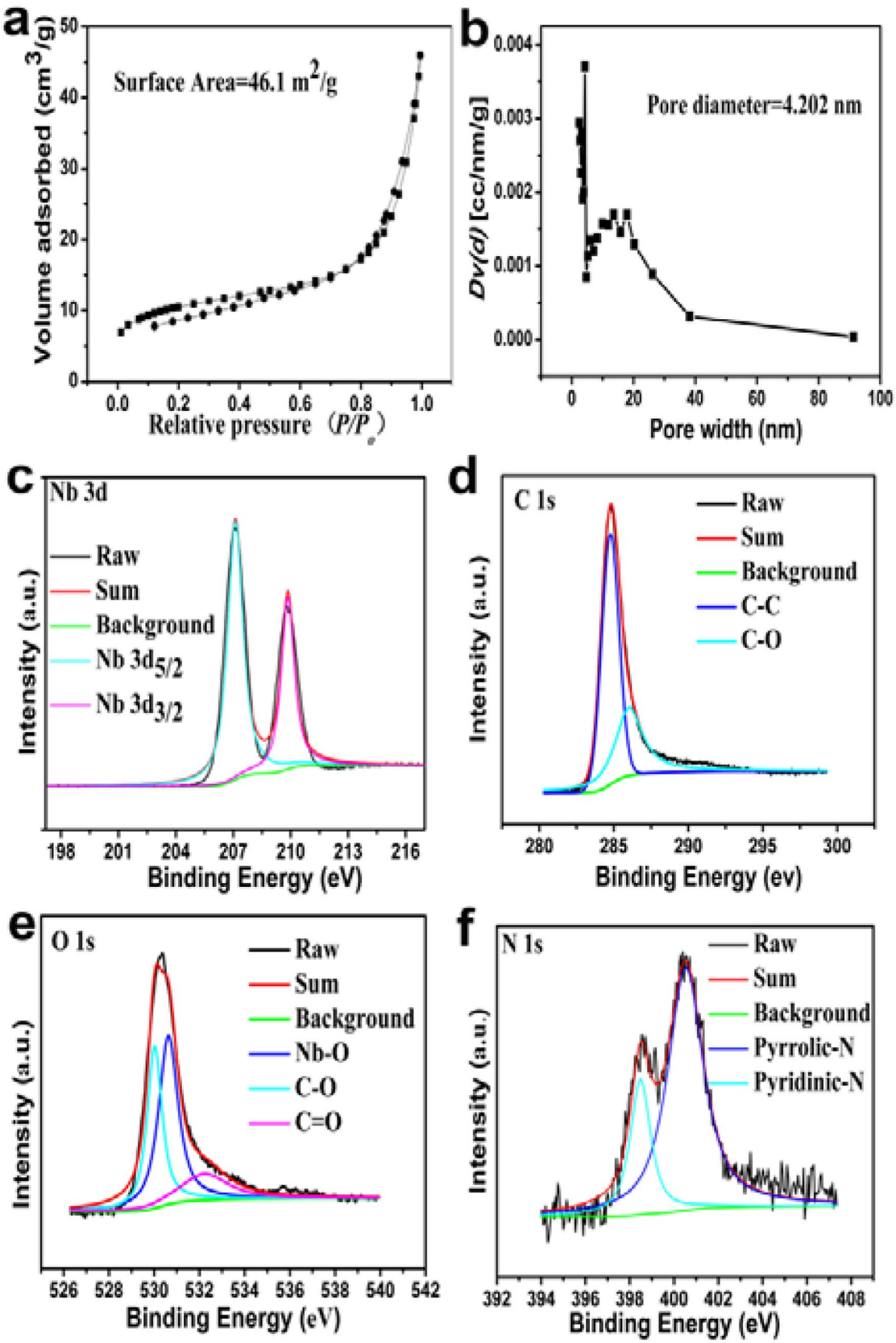

Fig. 2 **a** N_2 adsorption–desorption isotherm curve of Nb_2O_5/NC composites; **b** pore size distribution of Nb_2O_5/NC composites; **c**, **d**, **e**, **f** XPS spectra of **c** Nb 3d, **d** C 1 s, **e** O 1 s, and **f** N 1 s region for the Nb_2O_5/NC composites

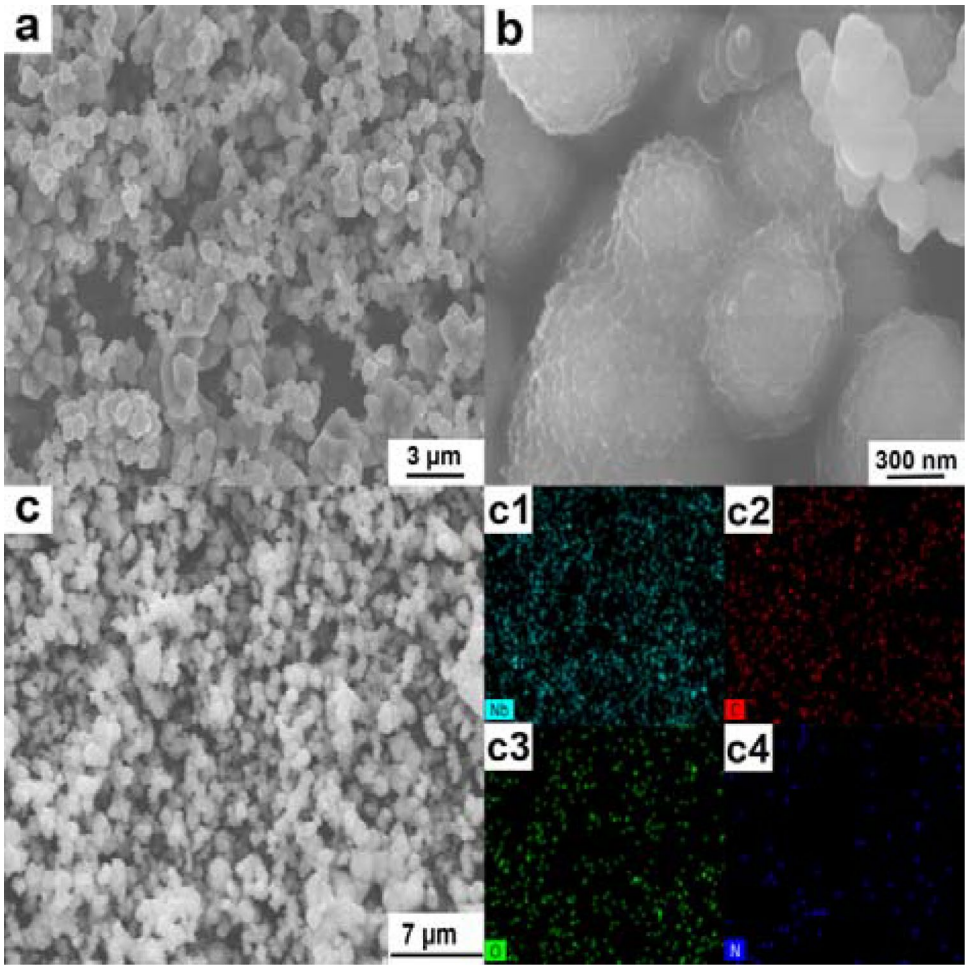

Fig. 3 **a**, **b** SEM images of Nb_2O_5/NC composites; **c**, **c1**–**c4** EDS mapping of Nb_2O_5/NC composites

much higher than that of Nb_2O_5. The battery capacity of Nb_2O_5/NC composite is 210, 182, 146, 112, 78, and 31 mAh g^{-1} at 0.1, 0.2, 0.5, 1.0, 2.0, and 5.0 A g^{-1}, respectively. When the current density recovers to 0.1 A g^{-1}, the battery capacity also recovers to 210 mAh^{-1}. It can be seen that the Nb_2O_5/NC composite material exhibits excellent rate capability.

The EIS measurement of Nb_2O_5/NC composites is performed for investigating the electrochemical kinetics. As shown in the Fig. 6a, b, the Nyquist plots of Nb_2O_5/NC and pure Nb_2O_5 contain arcs at high frequency and straight lines at low frequency, in which the semicircle corresponds to high-frequency region and the diagonal corresponds to low-frequency region. The diameter of the semicircle represents the charge transfer impedance; the larger the diameter of the semicircle means the larger the impedance. And the slope of the oblique line represents the ion diffusion impedance. The equivalent circuit diagram of Nb_2O_5/NC is shown in Fig. 6a, in which R1 and R2 correspond to solution resistance and transfer resistance, respectively. By contrast, it can be seen from Fig. 6a, b that the transfer resistance of Nb_2O_5/NC is less than that of Nb_2O_5 after 5 cycles and 20 cycles.

Furthermore, the Na^+ diffusion coefficients for the Nb_2O_5/NC and pure Nb_2O_5 electrodes were calculated according to formulas (1) and (2) [28–31]:

$$Z' = R + \delta_\omega \omega^{-1/2} \tag{1}$$

$$D = \frac{R^2T^2}{2n^4F^4\delta_\omega^2A^2c^2} \tag{2}$$

In the low-frequency region of the electrochemical impedance spectrum, the data were selected with Z' as the vertical coordinate and $w^{-1/2}$ as the horizontal coordinate to plot, and the slope was obtained after fitting (Fig. 6c). And then according to formula (2), get the diffusion coefficient (D_{Na+}). The diffusion coefficient (D_{Na+}) of Nb_2O_5/NC composite is 1.57×10^{-13} cm^2 S^{-1} and 7.55×10^{-13} cm^2 S^{-1} after 5 and 20 cycles,

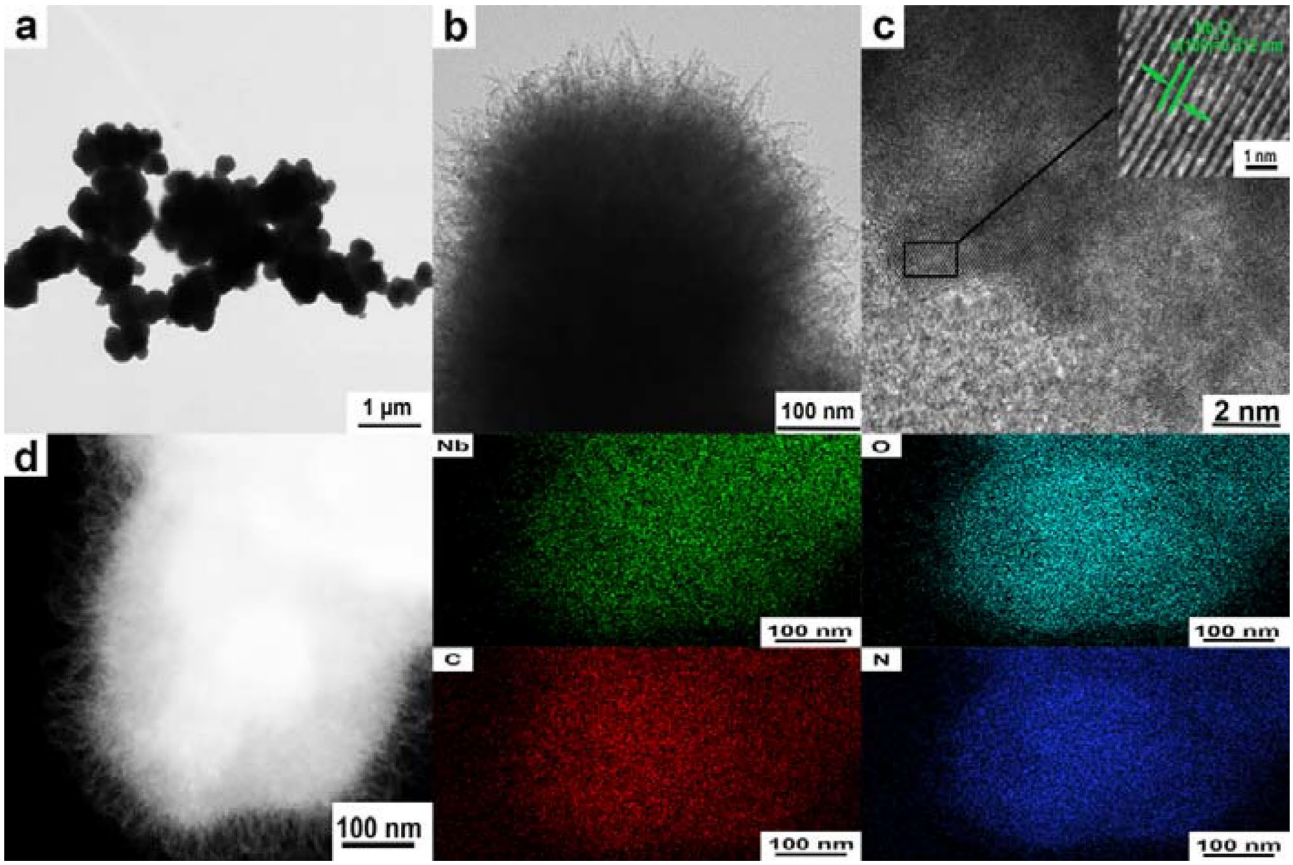

Fig. 4 **a**, **b** TEM image of Nb_2O_5/NC composites, **c** HRTEM image of Nb_2O_5/NC composites. **d** EDS mapping of Nb_2O_5/NC composite under transmission electron microscope

respectively, exceeding those for Nb_2O_5/C electrode (7.18×10^{-15} cm^2 S^{-1} and 2.76×10^{-13} cm^2 S^{-1} after 5 and 20 cycles).

To further explore the reaction kinetics of Nb_2O_5/NC composites, we performed CV tests on Nb_2O_5/NC composites at different scan rates (from 0.2 mV s^{-1} to 1.0 mV s^{-1}). As shown in Fig. 7a, an obvious peak shape appears from 0.4 mV s^{-1}, and the peak shape becomes sharper with the increase of the scan rate, that is, the faster the scan rate, the more serious the polarization. The *b* value is an important basis to judge the electrochemical reaction behavior of the diffusion-controlled process and pseudocapacitive behavior. When the *b* value is close to 0.5, it indicates that the diffusion behavior dominates the electrochemical reaction, and when the *b* value is close to 1.0, it indicates the pseudocapacitive contribution behavior [32]. The *b* value can be calculated according to the equation $\log i = b \log v + \log a$. As shown in Fig. 7b, the *b* values of the anodic peak 1 and cathodic peak 2 of the Nb_2O_5/NC composite electrode are corresponding to 0.9938 and 1.0292, which indicates that the redox process of the Nb_2O_5/NC composite electrode is a pseudocapacitive contribution behavior. The capacitive contribution can be calculated by the following equation: $i\,(V) = k_1 v + k_2 v^{1/2}$, where $k_1 v$ and $k_2 v^{1/2}$ represent the capacitive and diffusion capacities, respectively [8, 33]. Figure 7c is the CV map at 0.1 mVs^{-1}. It can be seen that the pseudocapacitive contribution behavior occupies 84.59% when the scan rate is 1 mVs^{-1}. Figure 6d shows the pseudocapacitive contribution ratio at scan rates of 0.2 mV s^{-1}, 0.4 mV s^{-1}, 0.6 mV s^{-1}, 0.8 mV s^{-1}, and 1.0 mV s^{-1}, which correspond to 70.98%, 74.60%, 78.88%, 82.15%, and 84.59%. It is obvious that as the scan rate increases, the pseudocapacitance contribution also increases. This means that the capacity of Nb_2O_5/NC composites at high scan rates is mainly related to pseudocapacitance, which provides a good proof for the superior rate capability of Nb_2O_5/NC composite electrodes.

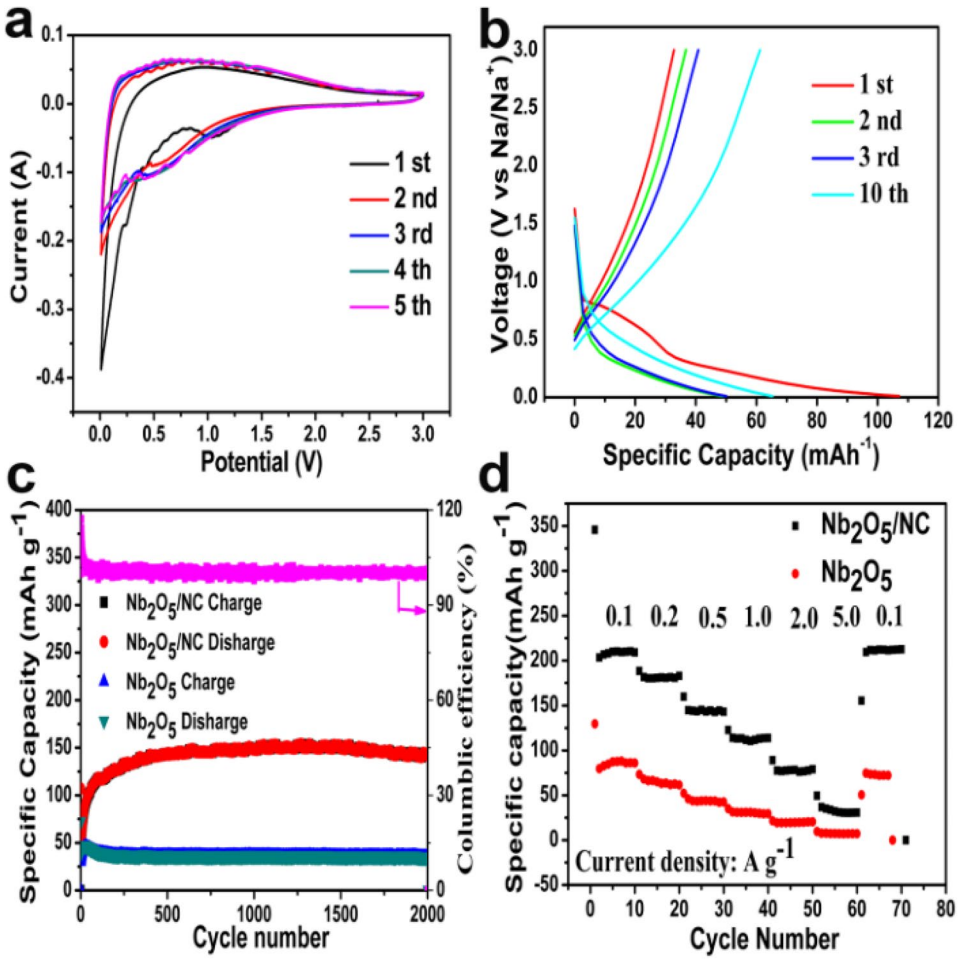

Fig. 5 **a** Cyclic voltammetry of Nb_2O_5/NC composites at 0.2 mV s^{-1} in SIBs; **b** charge and discharge curve of Nb_2O_5/NC composites at 1 A g^{-1} in SIBs; **c** cyclic performance of Nb_2O_5/NC composites and pure Nb_2O_5 at 1 A g^{-1} in SIBs; **d** rate capability of Nb_2O_5/NC composites and pure Nb_2O_5 in SIBs

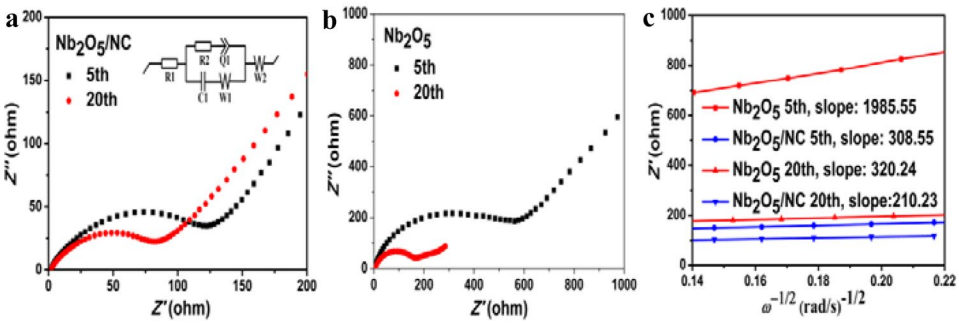

Fig. 6 **a**, **b** Electrochemical impedance test diagram of Nb_2O_5/NC composites and pure Nb_2O_5 in SIBs. (inset: equivalent electrical circuit for the fitting). **c** Plot of Zre with $w^{-1/2}$ in the low-frequency range for the electrodes made of Nb_2O_5/NC composites and Nb_2O_5 composites

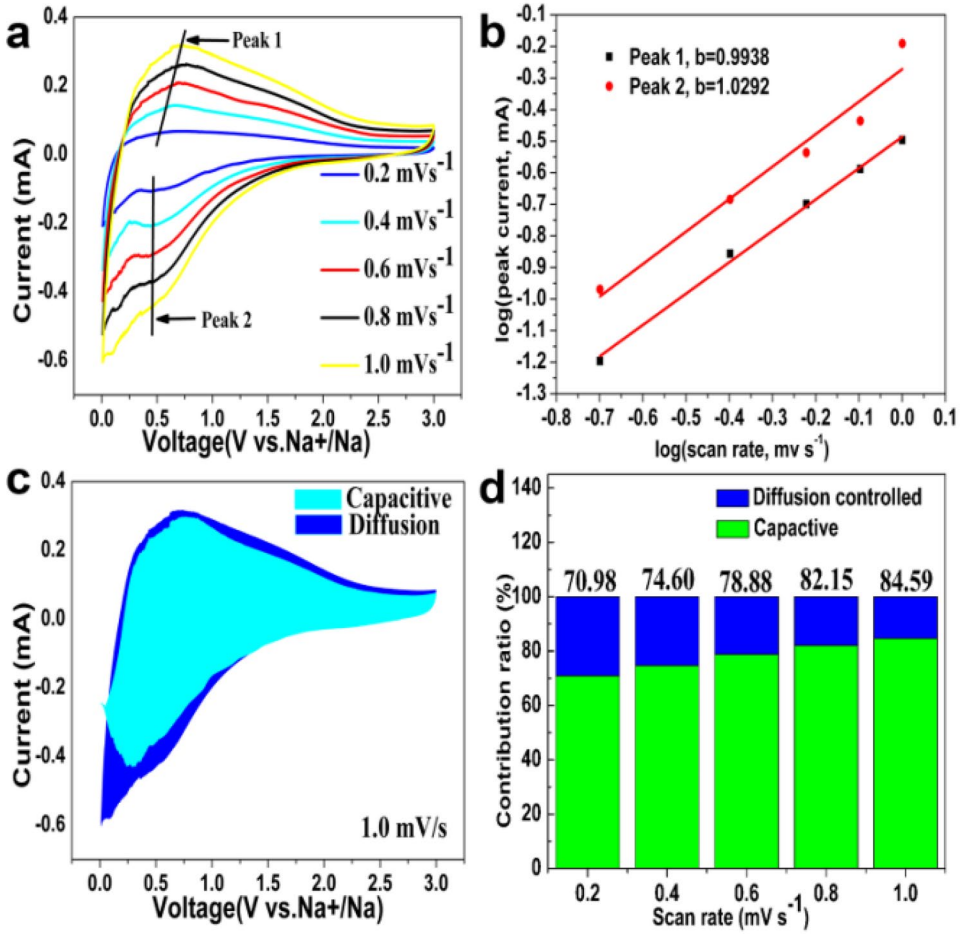

Fig. 7 **a** CV curves of the Nb_2O_5/NC composite electrode at different scan rates from 0.2 to 1.0 mV s^{-1}; **b** functional relationship of current response (*i*) vs. scan rate (*v*); **c** CV curves with the pseudocapacitive contribution to the total current shown by the shaded part at 1 mV s^{-1}; **d** bar chart showing the fraction of the pseudo capacitive contribution of the Nb_2O_5/NC composites electrode

Conclusion

In summary, a nano-solid spherical Nb_2O_5/NC composite was obtained by a single hydrothermal method followed by a calcination procedure. When Nb_2O_5/NC composite applied to the anode material of SIBs, it exhibited excellent cycling stability and rate capacity. The excellent performance of the Nb_2O_5/NC composite is ascribed to its unique nanosphere structure, in which Nb_2O_5 nanocrystals embedded in porous NC matrix can restrain agglomeration of Nb_2O_5 nanocrystals and ensure electrolyte accessibility, and the NC matrix can provide effective active sites and increase ions/electrons transfer. This study provides a rational approach for constructing high-performance Nb_2O_5-based electrodes as sodium-ion anodes with promising applications in large-scale energy storage.

Supplementary Information The online version contains supplementary material available at https://doi.org/10.1007/s10008-023-05515-9.

Funding This work is partially supported by the National Natural Science Foundation of China (No. 51764012, 21962002), the Foundation of Education Department of Jiangxi (GJJ211415), the Ganzhou Science and Technology Innovation Talent Plan (2020.60), the Natural Science Foundation of Jiangxi (20224BAB204024), and the Innovative Leading Talents of the Double Thousand Plan of Jiangxi Province (jxsq2019102045).

Declarations

Competing interests The authors declare no competing interests.

References

1. Lian S, Li G, Song F, Liu Z, Hu J, Tang K, Xie X, Wu Z, Zhang N (2022) Surfactant-free self-assembled MXene/carbon nanotubes hybrids for high-rate sodium- and potassium-ion storage. J Alloys Compd 901163426
2. Zhu Y, Hu Y, Qin C, Li Y, Yang Y (2022) Synthesis of free-standing N-doping Si/SiC/C composite nanofiber film as superior lithium-ion batteries anode. Mater Lett 306:130895
3. Palomares V, Serras P, Villaluenga I, Hueso KB, Carretero-González J, Rojo T (2012) Na-ion batteries, recent advances and present challenges to become low cost energy storage systems. Energy Environ Sci 5:5884–5901
4. Song J, Xiao J, Lin Y, Xu K, Li X (2018) Interphases in sodium-ion batteries. Adv Energy Mater 8:1703082
5. Li X, Lai W, Gan Y, He H, Yuan J, Zhang X, Yu H, Li X, Liu J (2022) Microstructures constructed by $MoSe_2$/C nanoplates

sheathed in N-doped carbon for efficient sodium (potassium) storage. J Alloys Compd 890:161746
6. Zhao Q, Whittaker AK, Zhao XS (2018) Polymer electrode materials for sodium-ion batteries. Materials 11:2567
7. Yuan J, Gan Y, Xu X, Mu M, He H, Li X, Zhang X, Liu J (2022) Construction of Fe_7Se_8@carbon nanotubes with enhanced sodium/potassium storage. J Colloid Interface Sci 626:355–363
8. Gan Y, He H, Mu M, Yuan J, Liao H, Li X, Yu Y, Zhang X, Liu J (2022) Fabrication of Bi_2Se_3/Mo_3Se_4 composite for efficient sodium storage. J Alloys Compd 923:166462
9. Ni J, Wang W, Wu C, Liang H, Maier J, Yu Y, Li LJ (2017) Energy storage: highly reversible and durable Na storage in niobium pentoxide through optimizing structure, composition, and nanoarchitecture. Adv Mater 29:1605607
10. Ni J, Li X, Sun M, Yuan Y, Liu T, Li L, Lu J (2020) Durian-inspired design of bismuth-antimony alloy arrays for robust sodium storage. Adv Funct Mater 14:9117–9124
11. Liu W, Yuan J, Hao Y, Maleki Kheimeh Sari H, Wang J, Kakimov A, Xiao W, Qin J, Li W, Xie C, Hu J, Peng J, Li X (2020) Heterogeneous structured $MoSe_2$-MoO_3 quantum dots with enhanced sodium/potassium storage. J Mater Chem A 8:23395–23403
12. Liu F, Cheng X, Xu R, Wu Y, Jiang Y, Yu Y (2018) Binding sulfur-doped Nb_2O_5 hollow nanospheres on sulfur-doped graphene networks for highly reversible sodium storage. Adv Funct Mater 28:1800394
13. Li H, Zhu Y, Dong S, Shen L, Chen Z, Zhang X, Yu G (2016) Self-assembled Nb_2O_5 nanosheets for high energy-high power sodium ion capacitors. Chem Mater 28:5753–5760
14. Fu S, Yu Q, Liu Z, Hu P, Chen Q, Feng S, Mai L, Zhou L (2019) Yolk–shell Nb_2O_5 microspheres as intercalation pseudocapacitive anode materials for high-energy Li-ion capacitors. J Mater Chem A 7:11234–11240
15. Zhang C, Beidaghi M, Naguib M, Lukatskaya MR, Zhao M-Q, Dyatkin B, Cook K, Kim S, Eng B, Xiao X, Long D, Qiao W, Dunn B, Gogotsi B (2016) Synthesis and charge storage properties of hierarchical niobium pentoxide/carbon/niobium carbide (MXene) hybrid materials. Chem Mater 28:3937–3943
16. Cao D, Yao Z, Liu J, Zhang J, Li C (2018) H-Nb_2O_5 wired by tetragonal tungsten bronze related domains as high-rate anode for Li-ion batteries. Energy Storage Mater 11:152–160
17. Kim Z, Lim E, Jo C, Yoon C, Hwang J, Jeong S, Lee S, Kang K (2015) Ordered-mesoporous Nb_2O_5/carbon composite as a sodium insertion material. Nano Energy 16:62–70
18. Meng J, He Q, Xu L, Zhang X, Liu F, Wang X, Li Q, Xu Q, Zhang Q, Niu C, Xiao Z, Liu Z, Zhu Z, Zhao Y, Mai Y (2019) Identification of phase control of carbon-confined Nb_2O_5 nanoparticles toward high-performance lithium storage. Adv Energy Mater 9:1802695
19. Vicentini R, Soares DM, Nunes W, Freitas B, Costa L, Da Silva LM, Zanin H (2019) Core-niobium pentoxide carbon-shell nanoparticles decorating multiwalled carbon nanotubes as electrode for electrochemical capacitors. J Power Sources 434:226737
20. Yuan J, Li X, Liu J, Zuo S, Li X, Fi L, Gan Y, He H, Xu X, Zhang X, Meng J (2022) Pomegranate-like structured Nb_2O_5/Carbon@N-doped carbon composites as ultrastable anode for advanced sodium/potassium-ion batteries. J Colloid Interface Sci 613:84–93
21. Hwang JY, Myung S, Sun Y (2017) Sodium-ion batteries: present and future. Chem Soc Rev 46:3529–3614
22. Li Y, Wang Y, Cui G, Zhu T, Zhang J, Yu C, Cui J, Wu J, Tan H, Zhang H, Wu Y (2020) Carbon-coated self-assembled ultrathin T-Nb_2O_5 nanosheets for high-rate lithium-ion storage with superior cycling stability. ACS Appl Energy Mater 3:12037–12045
23. Chen Z, Chen W, Wang H, Xiao Z, Yu F (2020) N-doped carbon-coated ultrasmall Nb_2O_5 nanocomposite with excellent long cyclability for sodium storage. Nanoscale 12:18673–18681
24. Yang H, Xu R, Gong Y, Yao Y, Gu L, Yu Y (2018) An interpenetrating 3D porous reticular Nb_2O_5@carbon thin film for superior sodium storage. Nano Energy 48:448–455
25. Liu W, Liu P, Mitlin D (2020) Review of emerging concepts in SEI analysis and artificial SEI membranes for lithium, sodium, and potassium metal battery anodes. Adv Energy Mater 10:2002297
26. Park J, Park S, Kim D (2020) High-power lithium-ion capacitor using orthorhombic Nb_2O_5 nanotubes enabled by cellulose-based electrospun scaffolds. Cellulose 27:9991–10006
27. El Hamaoui B, Zhi L, Wu J, Kolb U, Müllen K (2005) Uniform carbon and carbon/cobalt nanostructures by solid-state thermolysis of polyphenylene dendrimer/cobalt complexes. Adv Mater 17:2957–2960
28. Li R, Zhu X, Fu Q, Lian G, Chen Y, Luo L, Dong M, Shao Q, Lin C, Wei R (2019) Nanosheet-based $Nb_{12}O_{29}$ hierarchical microspheres for enhanced lithium storage. Chem Commum 55:2493–2496
29. Zhao S, Jia H, Wang Y, Ju N, Zhang X, Guo Y, Wang Y, Wang H, Niu S, Lu Y (2022) Engineering monodispersed 2 nm Sb_2S_3 particles embedded in a porphyrin-based MOF-derived mesoporous carbon network via an adsorption method to construct a high-performance sodium-ion battery anode. Dalton L 51:12524–12531
30. Liu W, Yuan J, Hao Y, Sari H, Wang J, Kakimov A, Xiao W, Qin J, Li W, Xie C (2020) Heterogeneous structured $MoSe_2$-MoO_3 quantum dots with enhanced sodium/potassium storage. J Mater Chem A 8:23395–23403
31. Zhang J, Wang J, Yu M, Ni J, Li L (2022) Understanding the role of topotactic anion exchange in the robust Cu ion storage of $CuS_{1-x}Se_x$. ACS Energy Lett 7:1835–1841
32. Long F, Xiang Y, Yang S, Li Y, Du H, Liu Y, Wu X, Wu X (2022) Layered manganese dioxide nanoflowers with $Cu^{2+}$and Bi^{3+} intercalation as high-performance cathode for aqueous zinc-ion battery. J Colloid Interface Sci 616:101–109
33. Wang X, Shen G (2015) Intercalation pseudo-capacitive $TiNb_2O_7$@carbon electrode for high-performance lithium ion hybrid electrochemical supercapacitors with ultrahigh energy density. Nano Energy 15:104–115